Methods based on hyperpolarization and flow for enhanced Magnetic Resonance

Patrick Berthault, Gaspard Huber

6. Methods Based on Solution Flow, Improved Detection and Hyperpolarization for Enhanced Magnetic Resonance

Patrick Berthault and Gaspard Huber

Université Paris-Saclay, CNRS, CEA, Nanosciences et Innovation pour les Matériaux, la Biomédecine et l'Energie, 91191, Gif-sur-Yvette, France

6.1. Introduction

Compared to other analytical [1] or imaging [2] techniques, Nuclear Magnetic Resonance (NMR) is a modality with an inherently low sensitivity, regardless of which spectroscopy (MRS) or imaging (MRI) is considered. Therefore, it is scarcely used to monitor rare or fugacious events. For instance, real operando MR is limited to only few domains, such as long-term analysis of the electrolyte degradation in batteries [3,4] or monitoring dynamic changes in the water concentration of fruit and stems [5]. To catch molecular systems in fast evolution, it is thus important to look for instrumentation and methods to increase either the mass sensitivity or the concentration sensitivity.

At a given magnetic field and sample temperature, instrumental ways to achieve NMR sensitivity gain can be sorted in three categories: i) spin flow, ii) cryo- and/or micro-detection, and iii) hyperpolarization.

In the first category, developed since the 80's, the idea is to constantly replace the nuclear spins saturated after radiofrequency excitation by new ones in the detection region. This is basically the principle of the white blood or time-of-flight (TOF) MRI angiography techniques, in which contrast between the static tissues and the flowing blood inside the vessels is enhanced by the spin motion [6]. Also, for analytical applications employing slowly-relaxing nuclei such as ^{13}C, closed-loop circuits are employed in which the solution is constantly renewed in the MRS detection area [7].

The second category deals with the optimization of the detection coil. Here we will only rely on the description of the classical induction-based methods to detect nuclear spins. It deals with reduction of electronic noise through temperature lowering

in cryocoils and high-superconducting coils, on the one hand, and, on the other hand, the reduction of the size of coils in order to increase the sensitivity for mass-limited samples [8].

The third category, hyperpolarization, which is the transient boost of nuclear polarization through transfer from a more ordered system, is more and more widely used. The main methods are optical pumping of noble gases (spin-exchange optical pumping, SEOP, and metastability-exchange optical pumping, MEOP), parahydrogen-induced polarization (PHIP) and dynamic nuclear polarization (DNP). Pros and cons of these techniques have been reviewed [9].

Some recent solutions aiming at combining two or three of these categories to reach even higher NMR sensitivity for the study of systems in operation are the subject of this chapter. After briefly recalling the theoretical and practical aspects of these methods, we focus on the MRI methods designed to optimally manage the out-of-equilibrium nature of hyperpolarization. Then we describe the instrumental developments using both flow and coil optimization, and those introducing hyperpolarization in complement to one of these two methods or both. Next, methods and setups for efficient dissolution of hyperpolarized species are reviewed. Finally, considerations are made on what could be an ideal system encompassing hyperpolarization, flow and optimized detection (remaining however on conventional NMR induction). We will illustrate the text with some figures arising from work performed in our laboratory.

6.2. Basics of the methods to increase NMR sensitivity

6.2.1. Spin hyperpolarization

The main richness of NMR, *i. e.* its non-perturbative and innocuous character due to the low energies involved, also leads to its main drawback, its lack of sensitivity. For a spin ½, the nuclear polarization at thermodynamic equilibrium (normalized population difference of the low energy level to the high-energy level) is given by the Boltzmann distribution law:

$$P = \frac{n_\downarrow - n_\uparrow}{n_\downarrow + n_\uparrow} = \tanh \frac{\gamma \hbar B_0}{2kT} \quad (6.1)$$

where γ is the gyromagnetic ratio and B_0 the magnetic field. This means that at room temperature, even in a magnetic field of 11.7 T, the proton nuclear polarization is only ca. 4. 10^{-5} (24999 spins on the high-energy level, 25001 on the other one). But nuclear spins have an advantage: they relax slowly (much slower than the electrons or the photons in any case), and therefore they can receive polarization from other – more ordered – systems.

Let us describe now the three main hyperpolarization methods, keeping in mind that there exist many other ones (Figure 6.1). The interested reader could for instance consult refs. [10] and [11] for a more complete description of them.

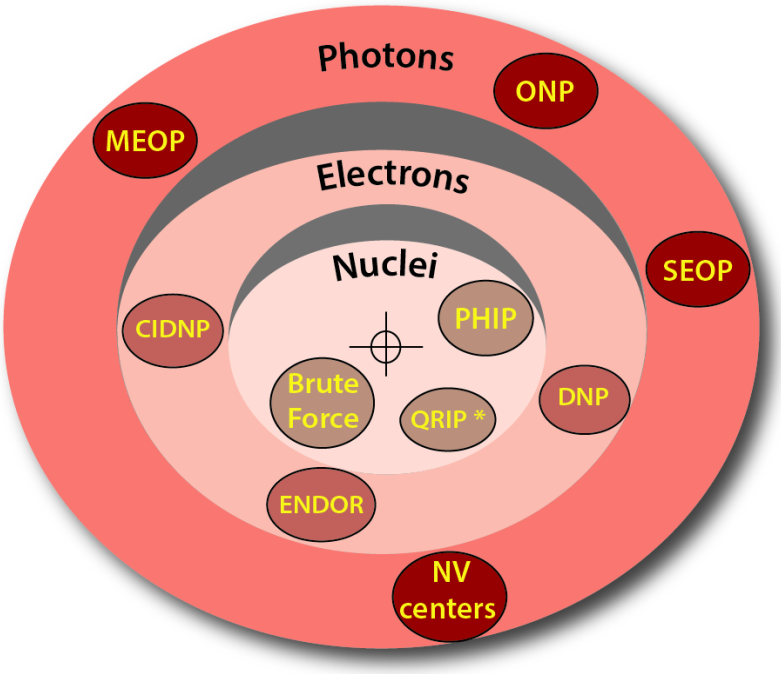

Figure 6.1 Main hyperpolarization methods. For details on the different techniques, see for instance the following references: Optical Nuclear Polarization - ONP: [12]; SEOP: [13]; MEOP: [14]; Nitrogen Vacancy - NV centers: [15]; DNP: [16]; Chemically-induced DNP - CIDNP (and photo-CIDNP): [17]; Electron-Nuclear Double Resonance - ENDOR: [18]; Quantum Rotor Induced Polarization - QRIP (* in fact correlations between rotational and nuclear spin states): [19]; PHIP: [10]; brute force: [20].

As electrons are fermions, they also obey the Boltzmann law. But due to a much higher ratio of their charge over their mass, their gyromagnetic ratio is ca. 700 times

higher than that of protons. Therefore in the DNP experiments using electrons as source of nuclear polarization a theoretical gain of 700 for the proton NMR signal can be expected. The work of Ardenkjaer-Larsen and co-workers has even demonstrated a much higher gain of a factor 10000 for dissolution-DNP [21]. The method consists in forming glassy matrices containing nuclei of interest and stable radicals. Nuclear spins are first polarized by the means of microwave irradiation at the electron spin transition frequency at low temperatures (≈ 1 K) and then the polarized sample is dissolved rapidly using a pressurized heated solvent and quickly transferred to the NMR spectrometer for data acquisition.

Ultimate gains of polarization could be obtained by transfer from photons. As they are bosons, they obey the Bose-Einstein distribution law, and it is well known that a photon beam can be fully circularly polarized (meaning that all photons have a spin +1 or -1). This is the basis of the optical pumping process. However, the situation is not so simple. Every nucleus in every molecule cannot be polarized in this way. First of all, the Zeeman levels responsible for the nuclear spin transitions are not isolated, and only particular atomic transitions can be excited by light. Second, for efficient optical pumping, an energy level not directly reached by the optical transition and which does not relax (or de-excite) too fast is required. Third, the relaxation of the target nucleus has to be considered. Taking all these into consideration, it follows that the most widely used optical pumping deals with noble gases of spin ½: ^{129}Xe and ^{3}He. For the former, spin-exchange optical pumping (SEOP) is the most commonly used method [13]. In SEOP, a circularly polarized light beam colinear to a magnetic field induces specific electronic transitions of alkali metal atoms, resulting in excess of population of one of the two electronic levels of the alkali metal ground state. Then, during collisions, spin exchange takes place between the alkali electron spins and the nuclear spins of the noble gas, resulting in its hyperpolarization. Although it is a quadrupolar nucleus thus experiencing faster relaxation, ^{83}Kr can also be hyperpolarized by this way. For ^{3}He, as it is a light atom with strict selection rules, the metastable 2 $^{3}S_1$ level (a singlet state) can be populated by a radiofrequency discharge. Then optical pumping occurs between the $^{3}S_1$ and $^{3}P_J$ sub-levels. In this method, which does not require the use of an alkali metal, nuclear polarization is transferred to ^{3}He atoms in the ground state via metastability-exchange collisions:

this is the principle of the metastability-exchange optical pumping (MEOP). Its quantum yield is excellent, but only low quantities of polarized nuclei per unit time are produced [22].

Saying that an ensemble is completely polarized is equivalent to defining it as being in a pure state. In the case of para-hydrogen, the molecules are in a pure singlet state, for which no NMR transition is possible. In the PHIP methods [23], the overpopulation of some nuclear spin states of protons is achieved through pairwise addition of the para-hydrogen nuclei on an unsaturated chemical compound, rendering them magnetically inequivalent. This hyperpolarization is then transferred to other nuclei mainly via scalar coupling. More recently, a parahydrogen-based method to hyperpolarize substrates in solution without modifying their chemical structure was proposed. The signal amplification by reversible exchange (SABRE) method was shown particularly useful to hyperpolarize molecules with heteroaromatic rings such as pyridine [24]. Not only MRS but also MRI may be performed using the SABRE method (Figure 6.2). Very recently, the method has been extended in order to hyperpolarize, in an aprotic solvent, virtually any molecule carrying an exchangeable proton [25].

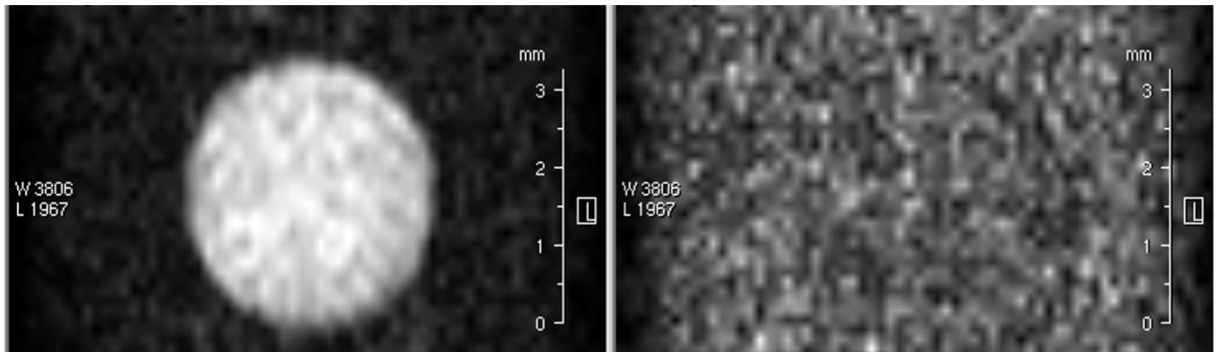

Figure 6.2 Axial ^{1}H Echo Planar Imaging of a solution containing pyridine (43 mM) and Crabtree's catalyst (2 mM) in a 5-mm NMR tube equipped with a J. Young's valve. Left: hyperpolarized through the dissolution of parahydrogen. Right: 40 seconds later. Slice: 4 mm; acquired points: 64 x 64 (theoretical resolution: 125 µm/point). Experiment time: 1s.

In all these hyperpolarization methods, the magnetic field value is highly important, both at the production place and for the transport and storage. For instance,

considering hyperpolarization via para-hydrogen in the 'irreversible' hydrogenative method, the magnetic field value and the process of transport to the NMR detection region will have an influence on the populated energy levels and therefore on the resulting ^{1}H spectra (basis of the PASADENA and ALTADENA methods, see for instance Chapter of C. R. Bowers in ref. [26] for detailed explanation). In the same vein, in the SABRE approach, the NMR methods to transfer polarization to the substrate of interest will not be the same at low and high magnetic fields [27]. Therefore in the conception and building of a system integrating hyperpolarization and NMR (micro)detection, these parameters will have to be taken into account.

6.2.2. Microcoils and cryocoils

Without consideration of the sample part, *i. e.* without taking into account the spin relaxation and susceptibility effects, the signal-to-noise ratio (SNR) of an NMR experiment is given by the following equation, initially expressed by Hoult and Richards [28] and reformulated here:

$$\mathrm{SNR} = \frac{k_0 \frac{B_1}{i} V_S N \gamma \hbar^2 I(I+1) \frac{\omega_0^2}{3\sqrt{2}kT_S}}{\sqrt{4(R_C+R_S)kT_C\Delta f}} \qquad (6.2)$$

In this equation, k_0 is a constant which accounts for the receiving coil geometry, V_S is the sample volume, N the number of spins per unit volume, γ the gyromagnetic ratio, I the spin angular momentum, ω_0 the Larmor frequency, T_s and T_c the sample and coil temperatures, R_s and R_c the sample and coil resistances, and Δf the receiver bandwidth.

The term B_1/i, the magnetic field per unit current, can be maximized by considering the Biot and Savart law. In the case of a single coil turn of radius r traversed by a current i, the law giving the magnetic field per unit current at its center is expressed as:

$$\frac{B_1}{i} = \frac{\mu_0}{2r} \qquad (6.3)$$

where μ_0 is the magnetic permeability of the free space. To get an idea of the order of magnitude, an electric current of 1 mA in a loop of 1 mm diameter would generate a field in the microtesla range.

As the reciprocity principle states that the signal received from a sample by a coil is proportional to the magnetic field which would be created in the sample if unit current was passed through the coil, the smaller the loop radius, the more sensitive the detection. As stated by Webb [8], the sensitivity gain by reduction of the coil diameter has to be tempered by the decrease of the sample volume (term V_s in Eq. 6.2). In conclusion, for mass-limited samples and a given coil volume, the best solution for optimal detection is when the space between the coil and the sample is as small as possible (highest filling factor).

Another important term in Eq. 6.2 is the coil temperature at the denominator, which explains the massive advent of cryogenic probes designed to reduce the thermal noise. Here, the thermal noise in the detection pathway, including the receiver coil, cables and preamplifier, is reduced by decreasing the temperature. However, since the sample remains at, or near room temperature, a thermal insulation is needed between the sample and the coil. This results in a reduction of the filling factor that decreases the signal. Overall, at the expense of a technologically more complex apparatus, the sensitivity gain of a cryo-detection system may reach a factor of 3 to 4 [29]. The resistance R_c of the coil and preamplifier can also be decreased using rf coils made of high-temperature superconducting materials [30, 31].

Various geometries of NMR coils have been proposed in the past. The advantages of each of them have been recently reviewed [32]. The widely used saddle coil geometry in commercial probes is not suitable for a down-scaling. Compared to planar microcoils, solenoid coils offer higher signal-to-noise ratio, but are more tedious to manufacture. Stripline coils [33] are very promising as they produce high and homogeneous B_1 field, a key parameter of the Hoult and Richards's equation, and show good scalability.

6.2.3. Solution flow

All ways to increase NMR sensitivity, *i. e.* intending to maximize the signal-to-noise ratio in a given period, are faced with the same observation. Most of the time spent in a classical pulse sequence is constituted by waiting delays. As between two experiments the interscan delay is designed to let the excited nuclear spins to return to equilibrium – or close to equilibrium - through longitudinal relaxation, it can become prohibitively large. This makes the NMR observation of some nuclei, particularly those with spin half and low gyromagnetic ratio, very cumbersome. This is the case for instance of ^{89}Y or ^{183}W in symmetrical environments (^{89}Y T_1 is larger than 600 s for YCl_3 in D_2O) [34], but also for less exotic nuclei, such as some quaternary ^{13}C and some ^{15}N. For instance, the ^{13}C T_1 in urea is ca. 40 s at room temperature, the ^{15}N T_1 values in acetonitrile and benzonitrile are on the order of a few minutes [35].

Obviously, such an issue may compromise not only the sensitivity of the NMR experiment, but also its capability to reproduce quantitatively the relative amounts of molecules in the sample, if the interscan delay is too short. To overcome such difficulties, for a long time it has been proposed to create a solution flow in a closed-loop circuit and to limit the NMR detection area to only a part of this loop [7, 36]. The use of paramagnetic species immobilized in another part of the circuit (outside the NMR detection area), designed to shorten the relaxation times of the nuclei of interest has also been suggested [37].

6.3. MRI methods dedicated to hyperpolarization

Hyperpolarized species can also be used to largely improve the spatial resolution in NMR images. In every MRI experiment, for a given field-of-view in one dimension, the intrinsic spatial resolution (in Hz/point) is given by the inverse of the highest value of the wave vector:

$$k_{max} = \gamma G_{max}\, t_{max} \tag{6.4}$$

Here G_{max} and t_{max} are the amplitude and duration of the gradient giving rise to the most distant point from the center of the k-space in this dimension, respectively.

The same rule applies for localized spectroscopy. For given excitation and/or inversion pulses, the size of each side of the voxel is also determined by $\gamma G_{max} t_{max}$. Here the maximal application time of the highest gradient in combination with the frequency selective pulse will give the thinner slice in the considered dimension.

But obviously other factors come to degrade this 'nominal' spatial resolution, such as diffusion, transverse relaxation or variation of the resonance frequency (due for instance to local magnetic susceptibility effects). It is also important to consider that diminishing the voxel size will decrease the signal-to-noise ratio, and it is for this last point that hyperpolarized species may become interesting.

Dealing with localized spectroscopy, firstly the gyromagnetic ratio is important. For instance, considering that $\gamma(^1H) = 3.61\ \gamma(^{129}Xe)$, the volume of the xenon voxel will be 47 times larger than that of the proton voxel for the same gradient strength.

Diffusion and relaxation should also be taken into account, but since we are focusing here on dissolved hyperpolarized species the self-diffusion coefficient values of which are close to those of the solvent molecules, they are of less influence than in the gas phase. Finally, the transient nature of the hyperpolarization imposes certain constraints on the recording of the NMR experiment. Preference will be given to pulse sequences that acquire the center of the k-space first.

For Cartesian sampling, this means using the centric encoding mode with alternation of the phase direction (0, $+\Delta G$, $-\Delta G$, $+2\Delta G$, $-2\Delta G$ …) or sampling only half the k-space. Note that according to the lifetime of the hyperpolarization with respect to the experiment time, a blurring may occur due to the decrease of the magnetization before the phase gradient from k-line to k-line in the phase dimension. To make the signal from hyperpolarization even more profitable, the transverse magnetization after each acquisition can be recycled (the condition here is that $T_2^* >> TR$). The Steady-State Free Precession (SSFP) experiments, which include the True Fast Imaging and Steady Precession (TrueFISP) sequence, are used to image hyperpolarized species and were particularly developed for ^{13}C [38]. The principle of such a sequence is based on the "rewinding" of the phase gradients in order to compensate for the displacement in the phase dimension of the k-space.

Non-Cartesian imaging methods like UTE, ZTE or SPIRAL could be preferred to Cartesian ones, but they may be more difficult to implement as prior knowledge of the k-space trajectories created by gradient shapes is necessary for data reconstruction. For the sake of sensitivity, on some systems the ^{1}H channel can be used to acquire these trajectories.

Dealing with localized spectroscopy, classical sequences such as PRESS or STEAM use many rf pulses for slice selection, a process rarely suitable for hyperpolarized species for the above-mentioned reasons. However, in certain circumstances, it is suitable to benefit from chemical exchange to perform fast, simple and sensitive spectroscopic imaging experiments. This is the case in the field of ^{129}Xe MRI-based pH sensors [39, 40]. In this approach, cage-molecules reversibly encapsulate hyperpolarized xenon, and give it specific spectral signatures at frequencies very different from that of free dissolved xenon, that resonates at ca. 200 ppm. A constant in-out exchange of xenon occurs with these systems. In a proof-of-concept experiment (Figure 6.3), it was shown that the simultaneous use of hyperpolarized xenon in two such xenon hosts possessing ionic groups enabled sensitive and bias-free measurement of solution pH. With the pulse sequence depicted in Figure 6.3b, free xenon is never excited, which enables us to keep xenon hyperpolarization for several minutes, according to its long T_1 value in D_2O. The xenon in-out exchange, slow with respect to the frequency difference between free and caged xenon, but fast with respect to the acquisition time, is used here to constantly replenish the small reservoir (caged xenon) in hyperpolarization.

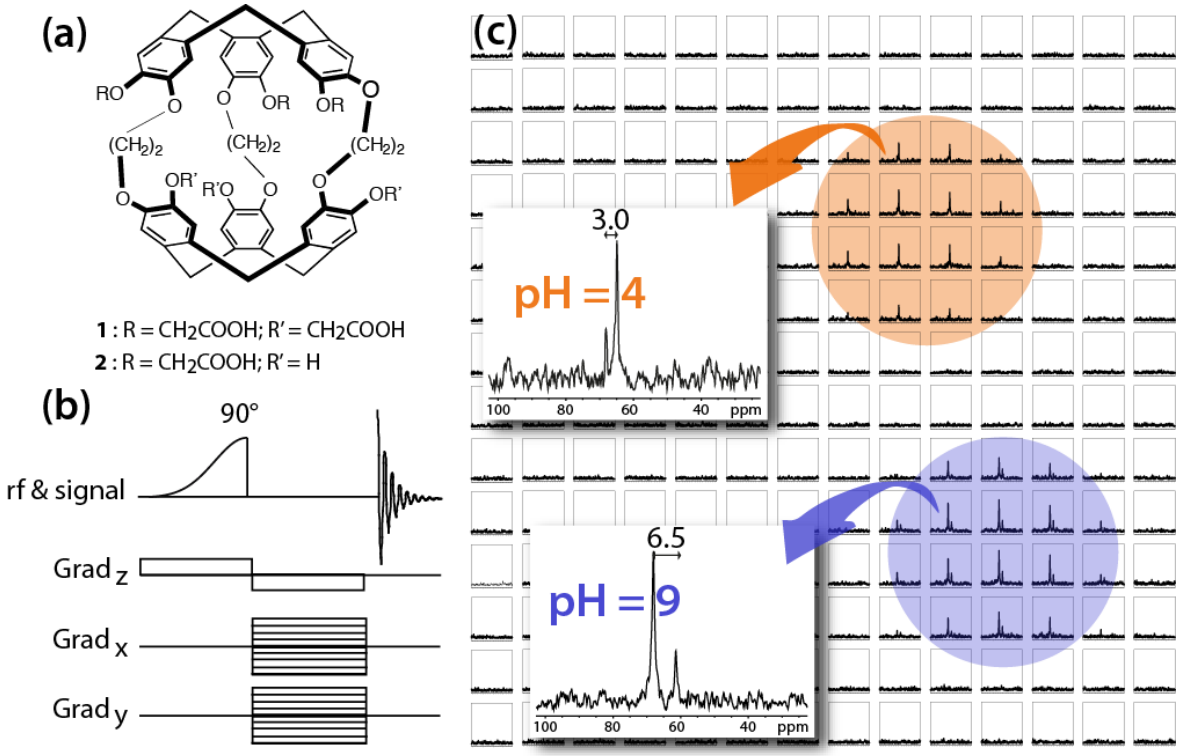

Figure 6.3 ^{129}Xe magnetic resonance spectroscopic imaging for pH sensing. Two tubes of 2.3 mm inner diameter contain a mixture of two cryptophanes (the xenon hosts) at pH 4 (orange) and pH 9 (purple), at concentrations between 150 and 250 µM. The experiment time was 53 s. (a) Structure of the two cryptophanes; (b) Pulse sequence, benefitting from in-out xenon exchange. The half-Gaussian soft pulse was centered on the Xe@cryptophane region, at ca. 60 ppm; (c) ^{129}Xe spectroscopic axial image with intrinsic spatial resolution of 500 µm per pixel. The chemical shift splitting gives access to the pH. Adapted from ref. [40] with permission from Wiley.

For detection of small amounts of analytes in such exchange regimes, it can also be advantageous to use indirect methods belonging to the Chemical Exchange Saturation Transfer (CEST) family. In 2006, the HyperCEST approach was proposed by Schröder et al. [41]. In this method, the rf saturation applied at the frequency of the small magnetization reservoir (caged xenon) leads to a decrease of the major signal, which is detected (Figure 6.4a). This enabled detection of picomolar substrate concentrations. The recording of a *Z*-spectrum (in which the main reservoir signal intensity is displayed as a function of the saturation frequency) however requires a very stable level of original hyperpolarization, which is not easy to obtain. For hyperpolarized species, it is more efficient to perform a spectrum-per-spectrum averaging than a point-per-point averaging. In this case, ultra-fast *Z*-spectroscopy

[42] can be advantageous (Figure 6.4b). In such a method, which has also been applied to DNP-hyperpolarized species, saturation is applied concomitantly with a pulsed field gradient. It amounts to saturate spins contained in a slice of the sample. Then, after the read pulse, detection follows in the presence of a second gradient, enabling the recording of the *Z*-polarization. By repeating the scan with and without saturation gradient, the *Z*-spectrum appears with high sensitivity.

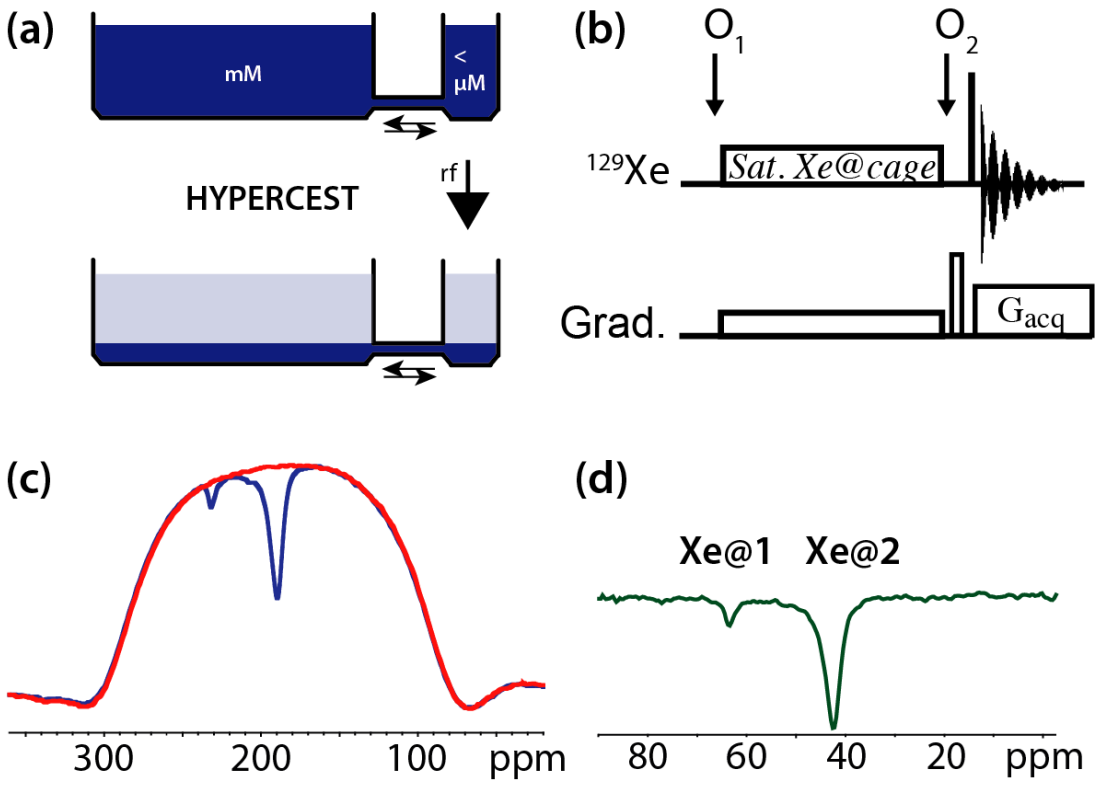

Figure 6.4 (a) Principle of the (Hyper)CEST spectroscopy. Saturation at the small pool frequency (xenon caged in cryptophanes for instance, signal around 60 ppm) will also decrease the large pool (free xenon, signal around 200 ppm) if the chemical exchange kinetics is appropriate. Adapted with permission from ref. [43]. Copyright (2003) American Chemical Society. (b) Pulse sequence used for ultrafast *Z*-spectroscopy. In each even scan, the minor xenon pool frequency is saturated at the O_1 frequency in the presence of a field gradient. Then the read pulse is applied at the resonance frequency of dissolved xenon O_2 (major pool). Detection is made in the presence of a second gradient. (c) In the absence of rf saturation the resulting ^{129}Xe spectrum displays the density distribution of xenon along the tube (red spectrum), whereas with saturation it reveals the presence of two xenon binding sites Xe@1 and Xe@2 (blue spectrum). (d) The difference between the two spectra provides the caged xenon signals. Adapted with permission from ref. [42]. Copyright (2013) American Chemical Society.

6.4. Combining methods to gain sensitivity

6.4.1. Flow and micro-detection

A reduction of the size of the NMR detection coil acts as an increase of the mass sensitivity. However, the sample preparation, *i. e.* the protocol for positioning the sample in the detection area while preserving its integrity and purity becomes increasingly tricky when the sample size decreases. In some examples, the sample was fixed with epoxy glues [44], embedded into an agarose gel [45], or confined to a particular area of a larger volume. But more often, a stopped flow system was used to position the sample precisely [46]. For example, a micro-fluidics system was conceived to position and analyze tiny samples. Here, individual worms and ova of typical dimensions around 0.1 mm were analyzed by ^{1}H NMR. The high sensitivity, of 2.5 10^{13} spin/Hz$^{1/2}$, allowed the detection of the most concentrated family of metabolites in the organisms [47].

On-flow analyses, in which the solution to be analyzed continuously flows in a channel that crosses the detection area during the analysis, offer the advantage that solutions may be hyphenated with other techniques. Decreasing the size of both the fluidic system and coil has several advantages in addition to an increase in mass sensitivity. Lower quantities of reactants and solvents are needed, a useful feature for optimizing chemical reactions. This is particularly advantageous when harmful chemicals are involved. Also, it reduces the time of homogeneous mixing of the reactants to values less than a millisecond, if the chamber is adequately designed [48]. This avoids the NMR analysis of an inhomogeneous solution that would not only broaden the signal by the local inhomogeneities resulting from the different magnetic susceptibilities of each fluid, but would also not account for the kinetics of the reaction that indeed occurs at the molecular scale. More valuable kinetic data and faster kinetics are therefore reachable. Finally, pressure and temperature are more easily controlled. This is particularly important for highly endo or exothermic reactions. A successful combination of flow and reduced dimensions of the mixing chamber and the detection coil to probe fast chemical reactions with the observation of intermediates has been exemplified [33]. Nevertheless, the flux mode has the disadvantage of broadening the NMR signals, simply because part of the solution leaves the detection coil during the time required for signal detection. Moreover,

when the flow rate is high, which is often required to probe fast kinetics, and when the reaction chamber is not submitted to the same magnetic field as the analysis chamber, the spin ensemble may not have the time to reach the Boltzmann equilibrium. Thus, as soon as longitudinal relaxation times differ, the peak integrals are no longer proportional to concentration. To counter this, a method, based on the use of the Bloch equations in a fluid dynamics simulation, has recently been proposed to quantitatively predict the transport of magnetization for any cell geometry and flow rates [49]. Nevertheless, the method requires the knowledge of longitudinal relaxation data. Placing several microcoils positioned along a capillary in which a reaction occurs has also been proposed to minimize the amount of needed reactants [50]. Remote detection is another elegant method to take advantage of the flow of the spins to be analyzed. Here, two coils are individually optimized. The spins are excited in the first coil, then stored as longitudinal magnetization as they flow toward a second coil used for detection [51]. The coupling of microcoils and flow finds applications e.g. in reaction monitoring and process control [48] but also in monitoring the metabolic answer in a living animal. For example, the fluctuation of lactate during neuronal simulation of a rat, using a homemade solenoidal microcoil, placed in the isocenter of an MRI scanner, has been demonstrated [52]. Here, the flow mode is used to perform a microdialysis, thus separating unwanted signals belonging to macromolecules or lipids from the signals of the small metabolites of interest, in the present case lactate.

As already mentioned, another setup for on-flow analyses is to use a closed-circuit for the solution, which has the advantage of requiring a smaller sample volume than in the open mode. In a recent development, the closed-circuit mode was combined with microcoil detection in a simple and disposable device made by 3D-printing [53]. It used the principle of a bubble mini-pump to induce circulation of the solution of interest in a small closed-loop circuit [54]. A significant gain of sensitivity was demonstrated when a solution of ^{13}C-enriched urea was analyzed by ^{13}C NMR spectroscopy compared to the static mode, *i. e.* when the solution does not circulate. Two versions of this setup were proposed. In the first one (Version 1 in Figure 6.5), the insert containing the fluidic channels and the NMR microcoil is electrically plugged onto a micro-imaging probe basis [53]. Two advantages are retained with

this version: i) it enables both spectroscopic and imaging experiments, ii) nuclei that are blinded in commercial probeheads can now be observed. Think for instance to ^{3}He or ^{205}Tl, with resonance frequencies higher than that of ^{31}P but lower than that of ^{19}F, a region usually not covered by commercial probeheads. However, such a setup has the inconvenience to be only adapted to a given commercial probehead basis (in the present case the Bruker micro-5 micro-imaging probe). Therefore, a second version (Version 2 in Figure 6.5) that uses inductive coupling between its microcoil and the coil of every NMR probehead has been proposed [55]. As for the open-circuit mode, a stopped-flow version results in a higher sensitivity than the on-flow alternative. When flow is abruptly stopped between each scan, all excited spins are detected during the full acquisition time.

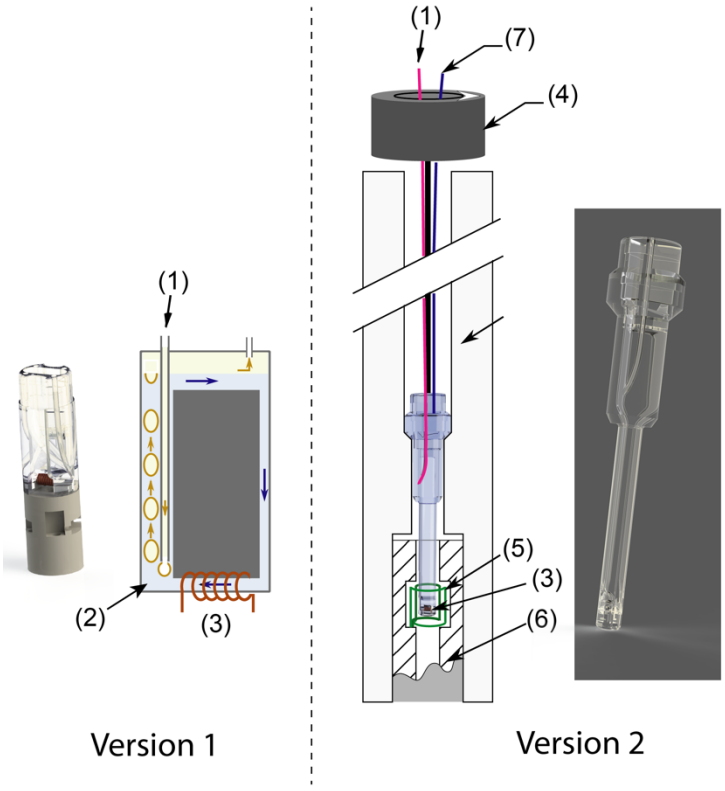

Figure 6.5 3D-printed NMR inserts combining flow of solution in a closed-loop circuit and micro-detection. (1): gas inlet; (2): solution of interest; (3): microcoil for NMR detection; (4): vernier placed on top of the magnet to manually optimize the inductive coupling; (5): coil of the host probe; (6): host probehead; (7:) second inlet tube for potential addition of other reactants. Reproduced from Ref. [53] and Ref. [55] with permission from The Royal Society of Chemistry.

In these two versions, a programmable syringe-pump pushes the carrier gas into the inlet channel (1) reaching the solution in the lower part of the insert. The bubbles that

are created are drawn upwards, which induces the flow of the solution (2). A solenoid microcoil (3) detects a part of the solution. Specifically, in version 2 of the insert (dubbed 'Wifi-NMRS'), a brass or plastic rod attached to the insert and ended by a vernier (4) ensures perfect axial alignment of the micro-solenoid with the coil (5) of the host probehead (6) to maximize the coupling between them. In these two setups, other inlet pipes can be added (7), for instance for introduction of reactants in the solution circuit. An advantage of these devices is that the solution circuit remains always in a magnetic field close or equal to that of the NMR detection area. This is important for quantitative results, as exemplified in Figure 6.6.

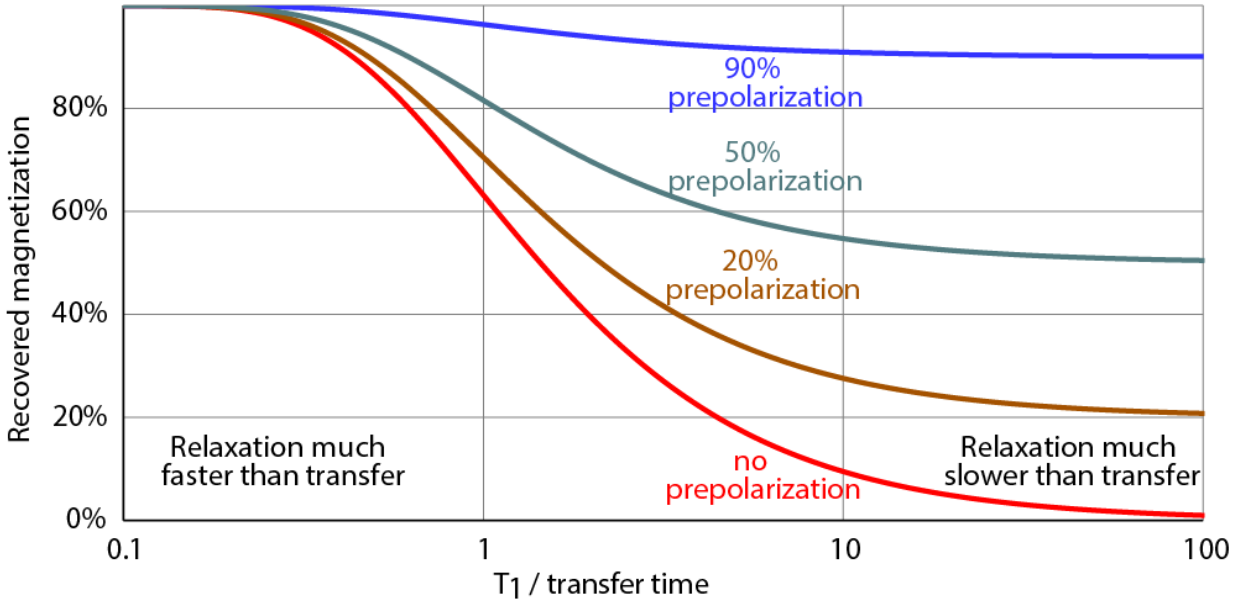

Figure 6.6 Amount of final magnetization as a function of the ratio T_1 over transfer time (sudden approximation) for a system where the sample is transported from the outside to the inside of the NMR detection area. As in the monitoring of synthesis intermediates the transfer time has to be as short as possible, the difference between the four curves shows the advantage of prepolarizing the sample.

6.4.2. Cryocoils and flow

The technologies needed for cryoprobes on one hand and flow on the other hand are a priori compatible. Thus, combining them should afford a significant advantage in term of sensitivity gain. Despite this, only a few achievements have been published. Schmidt et al. [56] used a hyphenated technique in which 20 compounds of comparable chemical structure at micromolar concentration were separated by liquid

chromatography. Then, while a small fraction was used for mass spectrometry analysis, which requires much less material than NMR due to its higher sensitivity, the large majority of the fractions were collected for concentration by solid phase extraction and then injected in stopped-flow mode to the NMR cell of a commercial 5-mm cryoprobe. ^{1}H spectra and COSY experiments, acquired within minutes to hours, allowed the identification of the majority of compounds.

Recently, another realization took advantage of flow to obtain a temporal resolution in the order of a few seconds [57]. Here, the reactants were introduced into a fixed-bed chromatographic reactor. The stationary phase was made of a catalytical bed that induced both the chemical reaction and the chromatographic separation. The solutes were detected in flow by using a commercial cryoprobe equipped with an home-made tube of 1 mm inner diameter. The tube diameter was reduced in order to avoid large distribution of the solute residence time values. However, it resulted in a lower filling factor of the cryoprobe, therefore decreasing the sensitivity of the analysis. The tube diameter had, therefore, to be compromised.

6.4.3. Hyperpolarization and micro-detection

Several reasons other than the increase in mass sensitivity alone may encourage the combination of spin hyperpolarization and microdetection (see Chapter 11 in ref. [58]). This can facilitate the conception of integrated systems encompassing hyperpolarization and NMR. In the case of a precious sample, the reduction of the quantity required for NMR analysis may also be mandatory. In addition, the use of small samples can be beneficial for microwave penetration in DNP experiments, or light penetration in photo-CIDNP ones. Finally, strong coupling between the sample magnetization and the detection system may provide a further gain in sensitivity.

6.4.3.1. Toward integrated mini-devices for hyperpolarization?

Hyperpolarized species can be produced either in the direct mode or in the batch mode, both methods having their pros and cons. Their 'on-flow' production enables to minimize relaxation issues, while being more difficult to setup: issues related to the lack of space, to the pollution of the sample (trace of alkali metal in the SEOP method for instance) may be encountered.

Regardless of the chosen production mode and the hyperpolarization method, the setup is usually bulky, not transportable and can hardly be integrated into a microfluidic platform that would contain NMR micro-detection. Very few studies have focused on reducing the size of these devices.

Jimenez-Martinez et al. designed an on-chip setup for xenon optical pumping which consisted of four chambers 1-mm thick and several millimeters wide connected by micro-channels [59]. A flow of xenon and quenching gas (such as nitrogen) passed from chamber to chamber. Each chamber also contained the alkali metal (rubidium). The second chamber received circularly polarized photons from the pump laser, while the third chamber received photons from the probe laser. A transverse DC field in the pump and probe chambers enabled the characterization of the ^{129}Xe polarization as a function of the total gas flow rate, alkali atomic density and pumping power. In this microtesla field, the NMR polarization of ^{129}Xe exceeded 0.5% at a flow rate of 5 ml/s.

Recently, it has been also shown how the use of microcoils and flows greatly brings decisive advantages to the development of the CIDNP technique [60]. In particular, the fact that the volume to be irradiated is only 1 microliter renders the use of a high-power laser for illumination obsolete. A sub-picomole detection limit has been demonstrated.

6.4.3.2. A further sensitivity gain in the non-linear regime

It is known for some years that intense magnetizations such as those created by optical pumping [61], para-hydrogen [62] or DNP [63] can lead to remarkable non-

linear effects (e. g. where the recorded signal is not directly proportional to magnetization), such a MASER or spectral clustering.

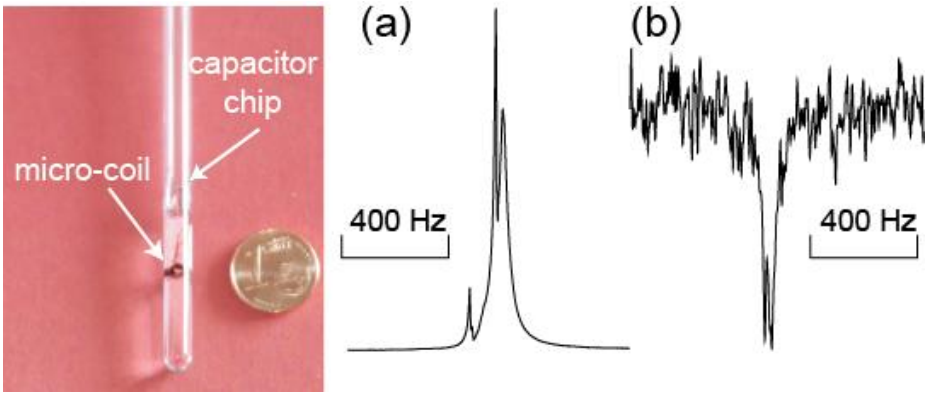

Figure 6.7 Laser-polarized ^{129}Xe spectra of a 5-mm NMR tube filled with a solution containing 8 mM ^{129}Xe. A microcoil is immersed in this solution. From left to right, the small peak corresponds to xenon in the hollow plug handling the microcoil, the narrow signal to the bulk phase, and the wider signal to xenon inside the microcoil. (a) After a small flip angle pulse. (b) Noise power spectrum. Adapted from ref. [64] with permission from Wiley.

These effects are maximized when the coupling between the magnetization and the detection system is optimized. In 2009, Desvaux *et al.* [64] performed the following experiment. In a 5-mm NMR tube, a micro-solenoid immersed in a solution was inductively-coupled to the ^{129}Xe channel of the NMR probehead. Xenon, previously hyperpolarized via spin-exchange optical pumping in batch mode, was introduced into the solution. It could be detected in a few minutes by classical NMR detection, but also by spin noise detection, *i. e.* without using rf excitation (see Figure 6.7). Remarkably, the spin noise detection favored the spins inside the microcoil. A sensitivity enhancement by a factor ≈ 50 was achieved by resorting to this inductively-coupled microcoil. The phenomenon that amplifies the spin-noise detection is the radiation damping characteristic rate, which can be expressed as [65]:

$$\lambda_r = \frac{\mu_0}{2}\eta Q \gamma \mathcal{M}_0 \tag{6.5}$$

Here η and Q are the filling factor and the quality factor of the probe, γ and $\mathcal{M}_0$ are the gyromagnetic ratio and the magnetization of the nuclear species of interest. This formula shows that both factors inherent to the detection system (filling factor and

quality factor) and to the hyperpolarization level (through the $\mathcal{M}_0$ term) are important to enhance the detection sensitivity. The microcoils, designed to exhibit high filling and quality factors, are thus perfectly suited to enhance these effects. Even for classical inductive detection, this non-linear regime [65] (the Bloch equations are no longer linear) assures that the resulting gain is higher than the simple factor of the gains due to hyperpolarization and to (micro-)detection. This may, however, be bought at the price of a loss of quantitative character if precautions are not taken.

6.5. Efficient dissolution of hyperpolarized species

Practical considerations on the use of hyperpolarized dissolved species in NMR have recently been reviewed [66]. Dealing with the use of hyperpolarized gases (or precursors of hyperpolarization for para-hydrogen), the conception of devices integrating both the mixing chamber and the detection part inside the cavity of the superconducting magnet may face several issues [58].

Firstly, these gases are poorly soluble in aqueous solvents, and in spectroscopy manual shaking of the NMR tube is often the best way to speed up their dissolution. The situation is worse for hydrogen, which is soluble only at the level of 0.8 mM/bar at 298 K [67], than for xenon or krypton, soluble at ca. 4.5 and 2.6 mM/bar, respectively, at the same temperature. This may lead to a lack of reproducibility, and it obliges one to consider the volume of hyperpolarized gas on top of the solution in the equations of state.

The use of hollow membranes with small pore sizes and high hydrophobic surface area is an elegant way to efficiently dissolve hyperpolarized species such as xenon and parahydrogen in solutions, under continuous flow conditions [66]. Baumer *et al.* introduced the concept using membranes made from polypropylene and with an average pore size of only 40 nm, to dissolve hyperpolarized xenon in blood with no observable loss of polarization [68]. Furthermore, these membranes were shown to be stable in other solvents such as DMSO and alcohols. Subsequently, the same hollow fiber membranes were successfully used to dissolve parahydrogen in an aqueous solvent [69].

6.5.1. Use of dissolved noble gases

The device presented in 6.4.1 was initially intended to introduce controlled quantities of optically-polarized xenon into the solution of interest (Figure 6.8) [54]. The specifications that led to the conception of this 3D-printed device were i) synchronizing the xenon introduction with the NMR pulse sequence, ii) avoiding the requirement of large volumes of solution, iii) avoiding the presence of bubbles in the NMR detection area that would degrade the field homogeneity. In this device, laser-polarized xenon, produced in the batch mode using a home-built SEOP polarizer, is separated from helium and nitrogen through cryo-condensation and stored in a glass coil on top of the NMR magnet. At this location, a field of 0.01 T is sufficient to prevent fast depolarization of the noble gas. In this setup, the role of xenon is double. Not only it enriches the solution in hyperpolarization but also it serves as a carrier gas to induce circulation of the solution in the closed loop. The design of the insert ensures that no bubble is present in the detection region, as proved by the ^{129}Xe spectrum displayed in Figure 6.8c.

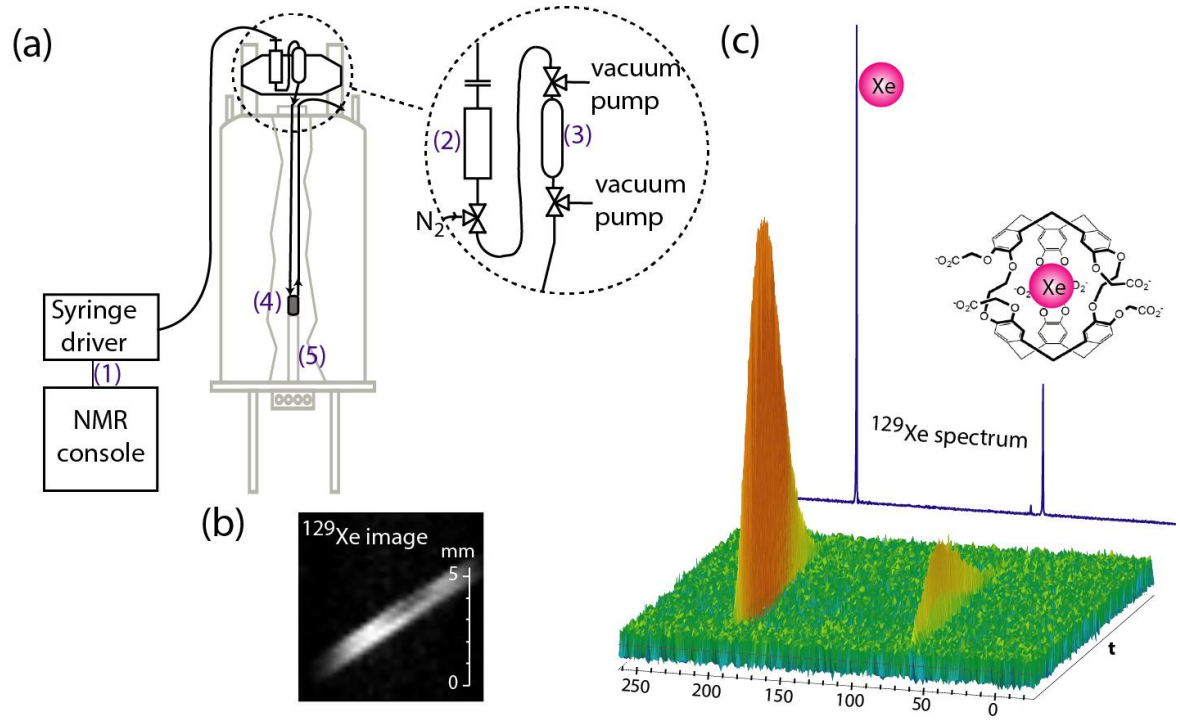

Figure 6.8 (a) Principle of the device delivering hyperpolarized xenon (produced in the batch mode) into the 3D-printed NMR inserts of Figure 6.5. A programmable syringe pump driven by the NMR console (1) pushes in a controlled way a buffer gas such as nitrogen (2), which itself pushes the hyperpolarized noble gas contained into the reservoir (3) toward the NMR

insert (4) plugged onto the NMR probehead (5). (b) ^{129}Xe axial image of the solution inside the microcoil. (c) ^{129}Xe NMR spectra obtained with this setup from an aqueous solution of cryptophane, as a function of time. The signal at ca. 70 ppm corresponds to xenon in the cage-molecule, the signal near 200 ppm to xenon free in solution. The absence of signal at 0 ppm indicates that there is no bubble in the detection region. Adapted from ref. [54] with permission from The Royal Society of Chemistry.

Such a device presents several advantages, e.g. being compatible with the use of hollow fiber membranes [70], and enabling both spectroscopy and imaging experiments with the same setup. However, as the initial setup was constrained by its electrical plugging to the basis of a given type of micro-imaging probehead, other versions using inductive coupling with the coil of every commercial probehead such as those presented in 6.4.1 have been built following the same principle [55].

6.5.2. Use of dissolved parahydrogen

Parahydrogen can also be suitable to flow applications and NMR detection by means of microcoils. Devices based on this association can reach an excellent sensitivity. A successful example concerns a system in which parahydrogen is introduced into a solution by means of a membrane included in a microfluidic chip [71]. The solution contains both the substrate to be hydrogenated and a suitable catalyst. Thanks to a detection volume of only 2.5 μl, picomole amounts of the substrate can be detected. Another device, based on high-field SABRE was recently proposed [*72*]. The head of an NMR probe designed for proton resonance at 500 MHz had been modified so that parahydrogen can diffuse in a liquid containing substrates responsive to SABRE and an appropriate catalyst. The liquid then flows through an NMR microcoil that serves both to excite spins by single excitation pulses, and detect them. Thanks to the presence of a co-substrate, the measurement of the concentration of substrates in the micromolar range was possible, based on a methodology developped by Eshuis et al. [73]. However modest enhancement factors were observed. SABRE is indeed known to be much less efficient at high-field than at lower field, being optimal around 0.01 T for protons. However, associating the proof of hardware concepts of this article and the recently proposed methods based on SABRE and efficient at high field [27], one would obtain a system combining sensitivity and dosage performances that

could result in interesting applications in health or food analysis applications, for example.

6.5.3. Dissolution-DNP

The detrimental effects associated with obtaining highly polarized samples via dissolution-DNP lies in the inherent paramagnetism linked to the presence of dissolved radicals. Several solutions, based mainly on the use of chemical scavengers to transform them into diamagnetic species [74] or using UV-generated, labile radicals [75], have been proposed.

6.6. Current status and perspectives

It is highly likely that the use of systems integrating hyperpolarization, solution flow and optimized detection will be expanded in the near future to exceed the current capabilities of liquid state NMR. Indeed, while hyperpolarization is mandatory to reach low detection thresholds, it can be of high interest to produce the hyperpolarized species very close to the place where they are detected, for several reasons: i) avoiding any human handling leads to a higher reproducibility, ii) the time between the production of these transient polarizations and their detection can be reduced, iii) synchronization between the injection of the hyperpolarized substance and the triggering of the pulse sequence can more easily be achieved. Thus in an ideal system provided to the chemist and aimed at quickly analyzing a mixture of liquids, the solution previously hyperpolarized would flow into an optimized detection area.

However, several limitations can be anticipated, mainly inherent to the out-of-equilibrium nature of hyperpolarized species in such a system. First, except maybe with DNP, not all nuclei of all molecules can be hyperpolarized. Second, the quantitative character of NMR may be lost, and ways have to be found to calibrate the amplitude of the response to the number of spins present.

Also, the issues that may be encountered when trying to integrate the polarizer and/or the mixing chamber inside or close to the NMR spectrometer depend on the hyperpolarization method.

For DNP, a difficulty may lie in the necessity to give access both to the micro-wave and the radiofrequency field to the same volume, without altering their individual performances (for a more detailed discussion, refer to Chapter 11 of ref. [58]). Thus, the most often encountered systems use the principle of sample shuttling. To this end either a device with two magnetic centers is used [76], or a magnetic tunnel designed to minimize relaxation during the sample transfer is built [77]. Conversely to what was described in 6.4.1 for non-hyperpolarized species, here the faster the transfer, the higher the resulting polarization and thus the NMR signal.

For optically-pumped noble gases, it is also important to keep them in (or very close to) the high magnetic field of an NMR spectrometer. Indeed, while optical pumping only requires a moderate magnetic field (in order to split the electron spin levels in SEOP for instance), the relaxation of a laser-polarized noble gas batch is accelerated when it diffuses in magnetic field gradients [13]. The best solution would be to place the optical cell inside the magnet bore, provided that the magnetic field gradients are not too high. Here anyway the main difficulty lies in the arrangement of the photon beam. While there exist optical fibers that can support high photon flux (keep in mind that the efficiency of the optical pumping is related to the number of photons that cross the optical cell, per unit time), they cannot maintain the light polarization. At their extremity the mixture of linear *s* and *p* polarization will be present, and, except if the magnetic field is high enough to expect discrimination of the transitions only through their frequency, a beam splitter cube and two quarterwave plates (one for each linear polarization) are required, which can become cumbersome. If the NMR system offers enough space, a solution with microfabricated chips can be proposed [59].

For PHIP, parahydrogen may be produced outside the magnet and delivered via tubing with slow isomerization, therefore keeping almost intact its capacity to induce hyperpolarization. However, as soon as parahydrogen is in contact with an appropriate catalyst in solution, the hyperpolarized signal decreases quickly at a rate defined by the longitudinal relaxation of the involved nuclei. So a system is needed in

which parahydrogen is quickly introduced in the solution, at, or near the region of homogeneous field in the core of the magnet, and the NMR spectra can quickly be recorded. An alternative is to use heterogenous catalysis, in which the solution containing dissolved hydrogen will flow through a solid phase catalyst. To do so, the device should fit with the available volume inside the NMR probe, in the core of the magnet, paying special attention to the parahydrogen dissolution process. The device proposed by Eills *et al.* [71] resolved two important challenges: accelerating parahydrogen dissolution by the use of a membrane, and increasing the pressure to increase the concentration of the dissolved gas. It uses a microcoil detector. In this article, the PASADENA hyperpolarization method gave intense signals, albeit in antiphase, and was limited to molecules comprising a multiple bond. Based on this kind of device, it would be profitable to apply other parahydrogen-based methodologies prone to produce high polarization levels at high magnetic field. Some molecules, such as pyruvate, may be produced in a hyperpolarized state based on the side arm methodology [78]. Also using the device with a SABRE methodology would extent the applicability to a large number of molecules. Various techniques of efficient SABRE at high field have been developed from which one is particularly promising when molecules with natural isotope abundance have to be quantitatively analyzed [79]. When coupled to a standard addition method, it gives accurate and reasonably precise concentrations of solute, even at micromolar concentrations. It would also be highly profitable to provide in phase signals, for instance using the SEPP concept [80]. Then, by adding to the NMR sequence an EXSY pulse scheme, chemical shifts of the molecules free in solution would be recovered. This would open the route toward the use of SABRE-Relay also at high field, a method developed so far only at low magnetic field, but applicable to the large panel of molecules comprising at least one exchangeable proton [25].

Finally, the use of cryocoils or high-temperature superconducting coils represents a gain of sensitivity that does not alter the other properties of NMR. Research to optimize instrumentation in combining micro and cryo aspects of the detection coil, as well as combining hyperpolarization methods with such devices, will probably become popular even with an apparently modest sensitivity gain. The success of probes equipped with cryocoils results from the absence of additional constraints for

the final user, which are neither instrumental nor a compromise with the previously cited qualities of NMR.

Acknowledgements

Support from the French Ministry of Research (project 17-LCV2-0002-01 LabCom DESIR, project ANR-19-CE19-0024 PHOENIX and project ANR-20-CE30-0021 HELPING) is acknowledged. Dr. V. Gervais (I2BC) is warmly thanked for reading the manuscript carefully.

References

1. Zhu Y, Fang Q. Analytical detection techniques for droplet microfluidics—A review. Analytica Chimica Acta. 2013;787:24- 35.
2. Shin T-H, Choi Y, Kim S et al. Recent advances in magnetic nanoparticle-based multi-modal imaging. Chemical Society Reviews. 2015;44:4501- 16.
3. Grey CP, Tarascon JM. Sustainability and *in situ* monitoring in battery development. Nature Materials. 2017;16:45- 56.
4. Ilott AJ, Mohammadi M, Chang HJ et al. Real-time 3D imaging of microstructure growth in battery cells using indirect MRI. Proceedings of the National Academy of Sciences of the United States of America. 2016;113:10779- 84.
5. Windt CW, Blümler P. A portable NMR sensor to measure dynamic changes in the amount of water in living stems or fruit and its potential to measure sap flow. Tree Physiology. 2015;35:366- 75.
6. Hartung MP, Grist TM, François CJ. Magnetic resonance angiography: current status and future directions. Journal of Cardiovascular Magnetic Resonance. 2011;13:19.
7. Sudmeier JL, Günther UL, Albert K et al. Sensitivity optimization in continuous-flow FTNMR. Journal of Magnetic Resonance A. 1996;118:145–56.
8. Webb AG. Radiofrequency microcoils for magnetic resonance imaging and spectroscopy. Journal of Magnetic Resonance. 2013;229:55- 66.
9. Lee JH, Okuno Y, Cavagnero S. Sensitivity enhancement in solution NMR: Emerging ideas and new frontiers. Journal of Magnetic Resonance. 2014;241:18- 31.
10. Hövener J-B, Pravdivtsev AN, Kidd B et al. Parahydrogen-based hyperpolarization for biomedicine. Angewandte Chemie International Edition. 2018;57:11140- 62.

11. Green RA, Adams RW, Duckett SB et al. The theory and practice of hyperpolarization in magnetic resonance using *para*hydrogen. Progress in Nuclear Magnetic Resonance Spectroscopy. 2012;67:1- 48.

12. Buntkowsky G, Hoffmann W, Kupka T et al. Application of optical nuclear polarization enhanced ^{13} C NMR. Journal of Physical Chemistry A. 1998;102:5794- 801.

13. Walker TG, Happer W. Spin-exchange optical pumping of noble-gas nuclei. Reviews of Modern Physics. 1997;69:629- 42.

14. Batz M, Nacher P-J, Tastevin G. Fundamentals of metastability exchange optical pumping in helium. In: Journal of Physics: Conference Series. IOP Publishing; 2011; 012002.

15. Suter D, Jelezko F. Single-spin magnetic resonance in the nitrogen-vacancy center of diamond. Progress in Nuclear Magnetic Resonance Spectroscopy. 2017;98- 99:50- 62.

16. Maly T, Debelouchina GT, Bajaj VS et al. Dynamic nuclear polarization at high magnetic fields. Journal of Chemical Physics. 2008;128:052211.

17. Goez M. Chapter 3 Photo-CIDNP spectroscopy. In: Annual Reports on NMR Spectroscopy. Elsevier; 2009. 77- 147.

18. Hoffman BM. Electron-nuclear double resonance spectroscopy (and electron spin-echo envelope modulation spectroscopy) in bioinorganic chemistry. Proceedings of the National Academy of Sciences of the United States of America. 2003;100:3575- 8.

19. Meier B, Dumez J-N, Stevanato G et al. Long-lived nuclear spin states in methyl groups and quantum-rotor-induced polarization. Journal of the American Chemical Society. 2013;135:18746- 9.

20. Hirsch ML, Kalechofsky N, Belzer A et al. Brute-Force Hyperpolarization for NMR and MRI. Journal of the American Chemical Society. 2015;137:8428- 34.

21. Ardenkjær-Larsen JH, Fridlund B, Gram A et al. Increase in signal-to-noise ratio of > 10,000 times in liquid-state NMR. Proceedings of the National Academy of Sciences of the United States of America. 2003;100:10158- 63.

22. Gentile TR, Nacher PJ, Saam B et al. Optically polarized ^{3}He. Reviews of Modern Physics 2017;89.

23. Kovtunov KV, Pokochueva EV, Salnikov OG et al. Hyperpolarized NMR spectroscopy: d-DNP, PHIP, and SABRE Techniques. Chemistry: an Asian Journal. 2018;13:1857- 71.

24. Adams RW, Aguilar JA, Atkinson KD et al. Reversible interactions with para-hydrogen enhance NMR sensitivity by polarization transfer. Science. 2009;323:1708- 11.

25. Iali W, Rayner PJ, Duckett SB. Using parahydrogen to hyperpolarize amines, amides, carboxylic acids, alcohols, phosphates, and carbonates. Science Advances. 2018;4:eaao6250.

26. Bowers, CR. Sensitivity Enhancement Utilizing Parahydrogen. In Encyclopedia of Nuclear Magnetic Resonance; Grant, DM, Harris RK, Eds.; Wiley: Chichester, U.K. 2002;9:750-69.

27. Barskiy DA, Knecht S, Yurkovskaya AV et al. SABRE: Chemical kinetics and spin dynamics of the formation of hyperpolarization. Progress in Nuclear Magnetic Resonance Spectroscopy. 2019;114- 115:33- 70.

28. Hoult DI, Richards RE. The signal-to-noise ratio of the nuclear magnetic resonance experiment. Journal of Magnetic Resonance. 1976;24:71- 85.

29. Kovacs H, Moskau D, Spraul M. Cryogenically cooled probes—a leap in NMR technology. Progress in Nuclear Magnetic Resonance Spectroscopy. 2005;46:131- 55.

30. Brey WW, Edison AS, Nast RE et al. Design, construction, and validation of a 1-mm triple-resonance high-temperature-superconducting probe for NMR. Journal of Magnetic Resonance. 2006;179:290- 3.

31. Laistler E, Poirier-Quinot M, Lambert SA et al. In vivo MR imaging of the human skin at subnanoliter resolution using a superconducting surface coil at 1.5 Tesla. Journal of Magnetic Resonance Imaging. 2015:41:496-504.

32. Gomez MV, de la Hoz A. NMR reaction monitoring in flow synthesis. Beilstein Journal of Organic Chemistry. 2017;13:285- 300.

33. Oosthoek-de Vries AJ, Nieuwland PJ, Bart J et al. Inline reaction monitoring of amine-catalyzed acetylation of benzyl alcohol using a microfluidic stripline nuclear magnetic resonance setup. Journal of the American Chemical Society. 2019;141:5369- 80.

34. Merritt ME, Harrison C, Kovacs Z et al. Hyperpolarized ^{89}Y offers the potential of direct imaging of metal ions in biological systems by magnetic resonance. Journal of the American Chemical Society. 2007;129:12942- 3.

35. Colell JFP, Logan AWJ, Zhou Z et al. Generalizing, extending, and maximizing nitrogen-15 hyperpolarization induced by parahydrogen in reversible exchange. Journal of Physical Chemistry C. 2017;121:6626- 34.

36. Laude DA Jr, Lee RWK, Wilkins CL. Signal enhancement of long-relaxing13C nuclei by flow NMR. Journal of Magnetic Resonance. 1984;60:453- 9.

37. Zhang Y, Laude DA. Immobilized free-radical substrates for magnetization of carbon-13 nuclei in flow NMR measurements. Journal of Magnetic Resonance. 1990;87:46- 55.

38. Golman K, Olsson LE, Axelsson O et al. Molecular imaging using hyperpolarized ^{13}C. British Journal of Radiology. 2003;76:S118- 27.

39. Berthault P, Huber G, Desvaux H. Biosensing using laser-polarized xenon NMR/MRI. Progress in Nuclear Magnetic Resonance Spectroscopy. 2009;55:35- 60.

40. Léonce E, Dognon J-P, Pitrat D et al. Accurate pH sensing using hyperpolarized ^{129}Xe NMR spectroscopy. Chemistry: A European Journal. 2018;24:6534- 7.

41. Schröder L, Lowery TJ, Hilty C et al. Molecular imaging using a targeted magnetic resonance hyperpolarized biosensor. Science. 2006;314:446- 9.

42. Boutin C, Léonce E, Brotin T et al. Ultrafast Z-spectroscopy for ^{129}Xe NMR-based sensors. Journal of Physical Chemistry Letters. 2013;4:4172- 6.

43. Zhang S, Merritt M, Woessner DE et al. PARACEST agents: modulating MRI contrast via water proton exchange. Accounts of Chemical Research. 2003;36:783- 90.

44. Peck TL, Magin RL, Lauterbur PC. Design and analysis of microcoils for NMR microscopy. Journal of Magnetic Resonance B. 1995;108:114- 24.

45. Grisi M, Vincent F, Volpe B et al. NMR spectroscopy of single sub-nL ova with inductive ultra-compact single-chip probes. Sci Rep. 2017;7:44670.

46. Seeber DA, Cooper RL, Ciobanu L et al. Design and testing of high sensitivity microreceiver coil apparatus for nuclear magnetic resonance and imaging. Review of Scientific Instruments. 2001;72:2171- 9.

47. Montinaro E, Grisi M, Letizia MC et al. 3D printed microchannels for sub-nL NMR spectroscopy. PLoS ONE. 2018;13:e0192780.

48. Liu Y, Jiang X. Why microfluidics? Merits and trends in chemical synthesis. Lab on a Chip. 2017;17:3960- 78.

49. Friebel A, Specht T, von Harbou E et al. Prediction of flow effects in quantitative NMR measurements. Journal of Magnetic Resonance. 2020;312:106683.

50. Ciobanu L, Jayawickrama DA, Zhang X et al. Measuring reaction kinetics by using multiple microcoil NMR spectroscopy. Angewandte Chemie International Edition. 2003;42:4669- 72.

51. McDonnell EE, Han S, Hilty C et al. NMR analysis on microfluidic devices by remote detection. Analytical Chemistry. 2005;77:8109- 14.

52. Crémillieux Y, Dumont U, Mazuel L et al. Online quantification of lactate concentration in microdialysate during cerebral activation using ^{1}H-MRS and sensitive NMR microcoil. Front Cell Neurosci. 2019;13:89.

53. Carret G, Berthelot T, Berthault P. Enhancing NMR of nonrelaxing species using a controlled flow motion and a miniaturized circuit. Analytical Chemistry. 2017;89:2995- 3000.

54. Causier A, Carret G, Boutin C et al.. 3D-printed system optimizing dissolution of hyperpolarized gaseous species for micro-sized NMR. Lab on a Chip. 2015;15:2049- 54.

55. Carret G, Berthelot T, Berthault P. Inductive coupling and flow for increased NMR sensitivity. Analytical Chemistry. 2018;90:11169- 73.

56. Schmidt S, Piechotta C, Godejohann M et al. Characterisation of commercially available linear alkylbenzenesulfonates by LC-SPE-NMR/MS (liquid chromatography-solid phase extraction-nuclear magnetic resonance spectroscopy-mass spectroscopy). Talanta.2010;82:143- 50.

57. Brächer A, Kreußer LM, Qamar S et al. Application of quantitative inline NMR spectroscopy for investigation of a fixed-bed chromatographic reactor process. Chemical Engineering Journal. 2018;336:518- 30.

58. Anders J, Korvink JG, Editors. Micro and nano scale NMR: Technologies and systems. Weinheim: Wiley-VCH; 2018.

59. Jiménez-Martínez R, Kennedy DJ, Rosenbluh M et al. Optical hyperpolarization and NMR detection of ^{129}Xe on a microfluidic chip. Nature Communications 2014;5:3908.

60. Mompeán M, Sánchez-Donoso RM, de la Hoz A et al. Pushing nuclear magnetic resonance sensitivity limits with microfluidics and photo-chemically induced dynamic nuclear polarization. Nature Communications. 2018;9:108.

61. Marion DJ-Y, Berthault P, Desvaux H. Spectral and temporal features of multiple spontaneous NMR-maser emissions. The European Physical Journal D. 2009;51:357- 67.

62. Suefke M, Lehmkuhl S, Liebisch A et al. Para-hydrogen raser delivers sub-millihertz resolution in nuclear magnetic resonance. Nat Phys. 2017;13:568- 72.

63. Chen H-Y, Lee Y, Bowen S et al. Spontaneous emission of NMR signals in hyperpolarized proton spin systems. Journal of Magnetic Resonance. 2011;208:204- 9.

64. Desvaux H, Marion DJY, Huber G et al. Nuclear spin-noise spectra of hyperpolarized systems. Angewandte Chemie International Edition. 2009;48:4341- 3.

65. Desvaux H. Non-linear liquid-state NMR. Progress in Nuclear Magnetic Resonance Spectroscopy. 2013;70:50- 71.

66. Berthault P, Boutin C, Martineau-Corcos C et al. Use of dissolved hyperpolarized species in NMR: Practical considerations. Progress in Nuclear Magnetic Resonance Spectroscopy. 2020;118- 119:74- 90.

67. Purwanto, Deshpande RM, Chaudhari RV et al. Solubility of hydrogen, carbon monoxide, and 1-octene in various solvents and solvent mixtures. Journal of Chemical & Engineering Data. 1996;41:1414- 7.

68. Baumer D, Brunner E, Blümler P et al. NMR spectroscopy of laser-polarized ^{129}Xe under continuous flow: a method to study aqueous solutions of biomolecules. Angewandte Chemie International Edition. 2006;45:7282- 4.

69. Roth M, Kindervater P, Raich H-P et al. Continuous ^{1}H and ^{13}C signal enhancement in NMR spectroscopy and MRI using parahydrogen and hollow-fiber membranes. Angewandte Chemie International Edition. 2010;49:8358- 62.

70. Simkins JW, Schuhmann S, Guthausen G et al. Characterization of biofilm distribution in hollow fiber membranes using compressed sensing magnetic resonance imaging. Journal of Membrane Science. 2020;594:117437.

71. Eills J, Hale W, Sharma M et al. High-resolution nuclear magnetic resonance spectroscopy with picomole sensitivity by hyperpolarization on a chip. Journal of the American Chemical Society. 2019;141:9955- 63.

72. Bordonali L, Nordin N, Fuhrer E, MacKinnon N, Korvink JG. Parahydrogen based NMR hyperpolarisation goes micro: an alveolus for small molecule chemosensing. Lab on a Chip. 2019;19:503- 12.

73. Eshuis N, Hermkens N, van Weerdenburg BJA et al. Toward Nanomolar Detection by NMR Through SABRE Hyperpolarization. Journal of the American Chemical Society. 2014;136:2695-8.

74. Miéville P, Ahuja P, Sarkar R et al. Scavenging free radicals to preserve enhancement and extend relaxation times in NMR using dynamic nuclear polarization. Angewandte Chemie International Edition. 2010;49:6182- 5.

75. Pinon AC, Capozzi A, Ardenkjær-Larsen JH. Hyperpolarized water through dissolution dynamic nuclear polarization with UV-generated radicals. Communications Chemistry 2020;3:57.

76. Leggett J, Hunter R, Granwehr J et al. A dedicated spectrometer for dissolution DNP NMR spectroscopy. Physical Chemistry Chemical Physics. 2010;12:5883-92.

77. Milani J, Vuichoud B, Bornet A et al. A magnetic tunnel to shelter hyperpolarized fluids. Review of Scientific Instruments. 2015;86:024101.

78. Reineri F, Boi T, Aime S. ParaHydrogen induced polarization of ^{13}C carboxylate resonance in acetate and pyruvate. Nature Communications. 2015;6:5858.

79. Eshuis N, Aspers, RLEG, van Weerdenburg BJA et al. 2D NMR trace analysis by continuous hyperpolarization at high magnetic field. Angewandte Chemie International Edition. 2015;54:14527- 30.

80. Eshuis N, Aspers RLEG, van Weerdenburg BJA et al. Determination of long-range scalar 1H–1H coupling constants responsible for polarization transfer in SABRE. Journal of Magnetic Resonance. 2016;265:59- 66.